Mode Selective Distributed Characterization of Few-Mode Fibers

Riccardo Veronese, Martina Cappelletti, *Student Member, IEEE/Optica*, Nicolas K. Fontaine, *Fellow, IEEE/Optica*, Haoshuo Chen, *Member, IEEE*, Mikael Mazur, *Member, IEEE/Optica*, Roland Ryf, *Fellow, IEEE/Optica*, Marco Santagiustina, *Member, IEEE*, Andrea Galtarossa, *Fellow, IEEE/Optica,* and Luca Palmieri, *Senior Member, IEEE/Optica*

***Abstract*—A new scheme for spatially resolved measurement of mode dispersion, modal birefringence and differential chromatic dispersion in few-mode fibers is presented and experimentally validated on a weakly-coupled, 4-mode-group fiber. The method relies on spectral correlation analysis between fiber's coherent Rayleigh backscattering traces generated by each of the supported mode groups, measured through optical frequency domain reflectometry. The presented technique provides a viable and effective way to measure modal and chromatic dispersion properties between arbitrary pairs of modes of the probed fiber, providing sub-picosecond delay resolution and centimeter-scale spatial resolution.**

***Index Terms*—Mode dispersion, chromatic dispersion, distributed measurement, Rayleigh scattering.**

I. Introduction

FEW-MODE fibers (FMF) are widely known as a space division multiplexing (SDM) capable transmission medium, where each of the supported modes is exploited as a transmission channel. In this context, the fiber's modal dispersion is a crucial parameter in the SDM system, as it plays an important role in the determination of the required DSP complexity at the receiver. Furthermore, in high symbol rate systems, the relative chromatic dispersion between the supported modes is another key feature to consider, as it significantly impacts the channel and is, therefore, important to measure.

Usually, the accumulated dispersion effects are characterized at the fiber end; several techniques are available to this aim, for both modal and chromatic dispersion, the majority of them being based on interferometric setups [1]–[3]. However, these non-distributed methods provide only aggregate information, making it impossible to localize irregularities or variations along the fiber. Recent advancements have introduced frequency domain methods capable of measuring group delay and chromatic dispersion for each mode in absolute terms without relying on fiber-specific mode multiplexers [4]. These approaches leverage vector network analyzers to extract the fiber's transfer function and decouple modal contributions mathematically. While effective, they are not distributed and require access to both ends of the fiber, limiting their ability to detect spatial variations or localized irregularities. Distributed characterization, based on the analysis of Rayleigh-backscattered light, addresses this limitation by enabling spatially-resolved measurements of key parameters such as differential group delay (DGD) and modal birefringence (MB). This is particularly advantageous for weakly-coupled FMFs, where uniform modal properties are essential for advanced applications like SDM [5], [6]. Distributed methods also achieve their maximum potential when applied to fibers spanning few kilometers, where variations or perturbations are more likely to occur along the length. This makes them essential for applications requiring precise fiber diagnostics in real-world scenarios. Recently, a method based on the spectral correlation analysis (SCA) of the coherent Rayleigh backscattering generated by the FMF has been introduced [7]. The method is based on optical frequency domain reflectometry (OFDR) and is able to measure along the FMFs both DGD and MB, i.e. the difference between the propagation constants, with spatial resolutions in the order of centimeters.

In this paper, we show how the SCA can be extended to characterize DGD and MB between arbitrary pairs of modes. Furthermore, we show how this technique can be exploited to measure also the relative chromatic dispersion between the modes composing the considered pair. The proposed method is experimentally validated on a weakly-coupled 4-mode-group step-index few-mode fiber [8], showing a very good agreement with the fiber's nominal properties.

II. From fiber's signature to modes' signatures

The SCA relies on the "signature" property of the fiber's coherent Rayleigh backscattering. Such a signal, despite its disordered appearance, is in fact a repeatable outcome of the specific distribution of Rayleigh scattering centers, peculiar to the fiber [9].

In silica glass fibers, the Rayleigh scatterers are embodied by density fluctuations, caused by the material's amorphousness. When shone with coherent light, each of these fluctuations acts as a reflector, scattering a small portion of the incident light back to the fiber's input; the signal resulting from the interference between all the backscattered contributions corresponds to the coherent Rayleigh backscattering of the fiber [10].

The easiest way to model the phenomenon is a discrete model [11], in which the Rayleigh backscattering is described

R. Veronese, is with Prysmian R&D, Viale Sarca 336, 20126 Milano, Italy M. Cappelletti, M. Santagiustina, A. Galtarossa and L. Palmieri are with the Department of Information Engineering, University of Padova, Padova, Italy. N. K. Fontaine, H. Chen, M. Mazur and R. Ryf are with the Nokia Bell Labs, New Providence, NJ, USA. A.G. and L.P. are also with CNIT – National Inter-University Consortium for Telecommunications, Italy. e-mail: martina.cappelletti.1@phd.unipd.it

Manuscript received December 26, 2024; revised December 26, 2024.

as being generated by a discrete distribution of scattering centers. In this scenario, the spectrum of the backscattered light can be written as

$$\hat{b}(\omega) = a(\omega) \sum_k \rho_k \exp\left(-j2\beta(\omega) z_k\right) \ , \tag{1}$$

where $a(\omega)$ is the input spectrum and the sum, representing the coherent superposition of the all the backscattered contributions, is performed over the whole set of scattering centers of the fiber; the quantities ρ_k and z_k, identifying respectively the reflection coefficient and the position of the k-th scatterer, are related to the distribution of density fluctuations traversed by the forward-propagating light.

Such a distribution is proper of each fiber, as it is determined by the random arrangement of its molecules happening during the quenching of the melted preform. As a consequence, two different fibers will be characterized by completely different distributions of scatterers, thus generating completely different (i.e., uncorrelated) backscattering signals. Furthermore, although being randomly placed, the scatterers are frozen within the fiber, unless a repositioning of its molecules is caused, e.g. by heating the fiber to melting temperature. As a consequence, in practical situations, the distribution $\{\rho_k, z_k\}$ of the scatterers can be considered as a fiber unique and immutable characteristic - its "signature".

However, being an interference signal, the shape of the coherent Rayleigh backscattering is affected also by another quantity, namely the propagation constant β. Indeed, as shown in (1), whenever β changes, so do the phase relations between the interfering contributions and thus the shape of the corresponding Rayleigh backscattering. Nonetheless, such a change is deterministic and results in a spectral shift.

The easiest way to understand this property is to note that in the expression for $\beta = \omega\, n/c_0$, the frequency ω and the effective refractive index n are factors of the same product, so that every variation Δn of n can be compensated by a specific frequency shift $\Delta f = \Delta\omega/(2\pi)$ such that

$$\frac{\Delta f}{f_0} \simeq \frac{\Delta n}{n} \ , \tag{2}$$

where f_0 is the carrier frequency. In other words, a variation Δn on the fiber's effective refractive index corresponds to a shift $\Delta f \simeq f_0 \Delta n/n$ of the backscattered spectrum. This spectral shift is directly linked to modal birefringence and thus to phase delay and effective refractive index. In addition to the spectral shift, the SCA also measures a temporal shift, which arises from differences in group velocity and is linked to the group index and chromatic dispersion. Together, these measurements enable the simultaneous characterization of both phase-related and group-related modal properties.

This principle was applied in [12] to analyze the DGD and birefringence of polarization-maintaining fibers using high-sensitivity OFDR. Building on this, a comparable approach was extended to study the modal properties, such as DGD and birefringence, in FMFs [7]. In this work, we further extend and refine this concept by introducing the notion of *modes' signatures of a fiber*, which allows a detailed characterization of mode-specific properties. Indeed, as the underlying distribution of the scatterers $\{\rho_k, z_k\}$ is the same for each mode, the backscattering signals generated by different modes in the same fiber can be considered (in first-order approximation) as frequency shifted versions of the same signature; moreover, according to (2), the shift Δf is proportional to the effective refractive index difference Δn (i.e. the MB) between the two considered modes. Furthermore, a time shift is also present between the two signals, as a consequence of the modes' different propagation speeds.

III. Mode-selective spectral correlation analysis

Distributed measurements are enabled by the fact that the aforementioned properties hold also in a local sense; in other words, the concept of signature still applies when we move from considering the whole fiber to one of its spans. According to this, the SCA works by cross-correlating the spectra of different sections of the fiber's Rayleigh time (space) trace in order to reveal a spectral correlation peak. Owing to the uniqueness property, the peak appears as soon as the two sections contain the signature of the same fiber span, i.e. they are spatially aligned for a specific mode-group pair.

In a single-mode scenario, a generic time span $\mathcal{T}_1 = [t_1, t_1 + T]$ of the backscattering signal has a one-to-one relation with the specific fiber section $\mathcal{Z}_1 = [z_1, z_2] = [t_1 v_g/2, (t_1 + T) v_g/2]$, where v_g is the mode's group velocity and the factor of two accounts for round-trip propagation. In this case, two arbitrary spans $\mathcal{T}_1 = [t_1, t_1 + T]$ and $\mathcal{T}_2 = [t_1 + \Delta t, t_1 + \Delta t + T]$, will spectrally correlate only if $\Delta t = 0$. Moreover, the correlation peak will be at $\Delta f = 0$.

Things change radically when we move to fibers supporting an higher number of modes. Consider the case of a fiber with two non-degenerate modes LP_i and LP_j [7]. In this case, due to the walk-off between the two modes, the generic time span $\mathcal{T}_1$ will be related to two different fiber sections, namely $\mathcal{Z}_{1,i} = [t_1 v_{g,i}/2, (t_1 + T) v_{g,i}/2]$ and $\mathcal{Z}_{1,j} = [t_1 v_{g,j}/2, (t_1 + T) v_{g,j}/2]$, where v_i and v_j are the different group velocities of modes LP_i and LP_j. In particular, owing to the linearity of the fiber, $\mathcal{T}_1$ will contain the superposition of the Rayleigh signatures generated in $\mathcal{Z}_{1,i}$ and $\mathcal{Z}_{1,j}$ respectively by mode LP_i and LP_j. Similar considerations apply to the delayed time span $\mathcal{T}_2$.

Assume now to perform SCA between $\mathcal{T}_1$ and $\mathcal{T}_2$; whenever the two corresponding fiber sections are *spatially* aligned, e.g. Δt is such that $\mathcal{Z}_{1,i} = \mathcal{Z}_{2,j}$, a correlation peak at a certain $\Delta f \propto \Delta n$ appears. However, in the presence of N co-propagating modes, a number of cross-correlations potentially equal to the number of mode pair combinations are generated. Outside their peak, these cross-correlations create background noise that decreases the already poor visibility of the peaks.

Therefore, the key point is to limit the number of simultaneously propagating MGs during the backscattering measurement. Nevertheless, the presence of different modes' signatures in the correlated sections is obviously a mandatory requirement for the SCA to be effective. To characterize several MGs while maintaining a high SNR, the solution is to

perform a mode-selective analysis, enabled by the invariance property of Rayleigh backscattering.

According to previous considerations, the distribution $\{\rho_k, z_k\}$ is a peculiar and immutable characteristic of every fiber. As a consequence, as long as the fiber is not perturbed - i.e. the effective refractive index n_i remains unaltered for each mode i, the mode's signature generated in a fiber span is invariant in time [9]. This suggests that the sections $\mathcal{T}_1$ and $\mathcal{T}_2$ subject to spectral cross-correlation can be selected on different backscattering measurements $b_1(t)$ and $b_2(t)$ of the same fiber; even then, the spectral correlation of two spatially aligned sections will reveal a correlation peak. In the case only mode i is propagating during measurement $b_1(t)$ and mode j during measurement $b_2(t)$, the highest SNR in characterizing the mode pair (i, j) is achieved. We recall that the only requirement is for the fiber to remain unperturbed between the two correlated measurements.

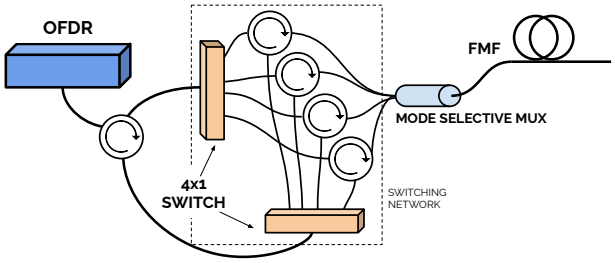

Fig. 1. Experimental setup. An OFDR system is connected to a switching network and a mode selective multiplexer. The optical circuit, composed of 4×1 switches, circulators, and a fan-in, allows for the selection of different MGs for launching into the FMF.

To achieve this, a setup like the one shown in fig. 1 can be implemented. An OFDR is equipped with a switching network and a mode selective multiplexer (e.g. a photonic lantern), allowing the selection of the launched MG without perturbing the fiber. The fiber's signature generated by each MG can therefore be collected by consecutive measurements while the fiber remains in a stable state. Subsequently, the SCA can be performed between different measurements, revealing the dispersion properties of the selected mode pair. Whenever this scheme is implemented, the only limit resides in the *spatial* similarity of the correlated MGs. Indeed, the spectral shift property holds only in first approximation when dealing with signatures of non-degenerate modes; in reality, a signature depends also on the spatial distribution of the generating mode. As a consequence, modes having very different field distributions can lead to faint spectral correlation peaks.

The scheme reported in 1 was designed for a 4-mode FMF; however, it can be straightforwardly extended to a N-mode fiber exploiting 2 Nx1 switches and N circulators. A generic measurement performed by such a scheme can be identified by a the notation $\mathrm{LP}_i \rightarrow \mathrm{LP}_j$, where the first element corresponds to the port through which the probing light is injected in the fiber, while the second one refers to that from which the Rayleigh scattering is measured.

IV. Measuring Mode Dispersion

As introduced in the previous section, the SCA principle is that to cross-correlate the spectra of two different sections $\mathcal{T}_1$ and $\mathcal{T}_2$ of a coherent Rayleigh measurement; in [7], the two sections were selected on the same measurement $b(t)$, during which multimode propagation was happening. Conversely, in this case, the SCA algorithm takes sections $\mathcal{T}_1$ and $\mathcal{T}_2$ respectively from measurements $b_1(t)$ and $b_2(t)$; to characterize the dispersion of LP_j with respect to mode LP_i, measurement $b_1(t)$ must contain the signature of mode LP_i while $b_2(t)$ that of mode LP_j. Owing to the mode selectiveness of the exploited multiplexer, the best choice to this aim is to set the measurement $\mathrm{LP}_i \rightarrow \mathrm{LP}_i$ as $b_1(t)$ and $\mathrm{LP}_j \rightarrow \mathrm{LP}_j$ as $b_2(t)$.

At this point, the SCA algorithm works by selecting consecutive sections $\mathcal{T}_1 = [t_i, t_i + T]$ on $b_1(t)$, and spectrally cross-correlate them with sections $\mathcal{T}_2 = [t_i + \Delta t, t_i + \Delta t + T]$ of $b_2(t)$, taken for different values of Δt. In order for the procedure to be effective, the two measurements must be referred to the same absolute time axis, so that the two OFDR scans have to be performed over the same optical bandwidth $\mathcal{B}$. The outcome of this procedure is the volumetric dataset $C(t, \Delta t, \Delta f)$, representing the modulus of the cross-correlation value at Δf, when section $\mathcal{T}_1$ starts at t and section $\mathcal{T}_2$ is shifted of Δt with respect to it. If a polarization-diverse receiver is implemented in the OFDR, the SCA can be performed for every possible combination of measured polarization states, so that the outcome becomes $C(p, t, \Delta t, \Delta f)$, p corresponding to one out of four possible combinations. Nonetheless, a polarization-independent dataset can be obtained by taking the maximum of C with respect to p, obtaining $C'(t, \Delta t, \Delta f)$. We recall that, if a significant correlation peak occurs at a specific point of coordinates $(t, \Delta t, \Delta f)$, then it means that at position $z \approx c_0 t/(2n_0)$ two modes (LP_i, LP_j) are experiencing a modal birefringence equal to $\Delta n_{i,j} = n_0 \Delta f / f_0$, f_0 being the central frequency of the OFDR scan, and a round-trip DGD equal to Δt; note that all the extracted quantities depend on the choice of a reference refractive index n_0.

The distributed information about the cumulated DGD can be revealed taking the maximum of C' with respect to Δf. On the other hand, local MB information can be extracted taking the maximum of C' with respect to the Δt axis.

This analysis is governed by two main parameters, namely the OFDR scan bandwidth $\mathcal{B}$ and the SCA window length L. $\mathcal{B}$ directly determines the sampling period $\delta t = 1/\mathcal{B}$ with which the Rayleigh signal $b(t)$ is recorded, and corresponds to the lower limit of the measurable cumulated DGD. On the other hand, the window length L determines the spatial resolution of the measurement as well as the resolution δn on Δn through the frequency resolution δf of the cross-correlation, being equal to $\delta f = \mathcal{B}\delta z / L = f_0 \delta n / n_0$.

In this case, the measurements were performed by means of a custom OFDR setup developed by the Nokia Bell Labs [3]; the optical bandwidth $\mathcal{B}$ was set to roughly 8.5 THz, corresponding to $\delta t = 118$ fs or, equivalently, to a spatial sampling step $\delta z = c_0/(2n_0\mathcal{B}) = 12$ µm. The window length

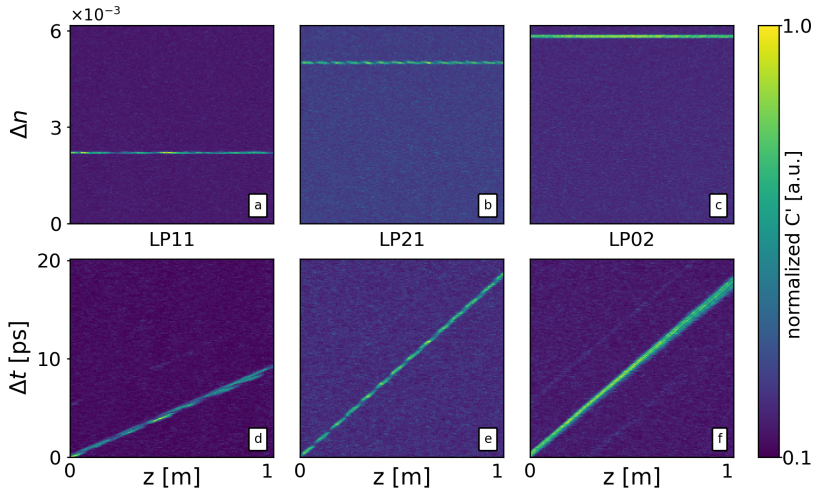

Fig. 2. Modal dispersion properties of the fiber with respect to the LP_{01} mode group. Each column corresponds to a mode group LP_j; the related plots have been obtained from the SCA outcome $C'(t, \Delta t, \Delta f)$ between measurements $LP_{01} \rightarrow LP_{01}$ and $LP_j \rightarrow LP_j$. Subplots (a)-(c) have been obtained as $\max_{\Delta t} C'(t, \Delta t, \Delta f)$. Subplots (d)-(f) as $\max_{\Delta f} C'(t, \Delta t, \Delta f)$. Modal birefringence and DGD are reported on the y-axis of the first and second row subplots respectively. Distance along the fiber is reported on the x-axis on all the subplots. The columns of each subplot in fig. 2 have been normalized by their mean value; each obtained plot have been then normalized to its own maximum.

L was set to roughly 2 cm, leading to a resolution Δn on the MB equal to $\Delta n = 3.1 \cdot 10^{-5}$.

The new scheme has been tested on a 1 m sample of a weakly-coupled, step-index 4-mode-group FMF [8], supporting LP_{01}, LP_{11}, LP_{21} and LP_{02} mode groups; the fiber has been equipped with a mode-selective photonic lantern [13] and connected to the switching network. The measurements of the modes' signatures have been carried out consecutively and as fast as possible, in order to rule out any effect brought by environmental fluctuations. The exploited lantern allows for the selection of the two degenerations a-b of modes LP_{11} and LP_{21}; as a consequence, the SCA outcomes C' related to the two degenerations of the same mode have been merged together taking the point-wise maximum, in order to obtain a single outcome C' for each mode group.

To perform a complete characterization of the mode dispersion properties of a FMF it is sufficient to measure DGD and MB for each mode group with respect to a fixed reference one. Figure 2 shows the results of the above analysis, performed using $LP_{01} \rightarrow LP_{01}$ as the reference measurement $b_1(t)$. The first row (Fig. 2a-c) refers to the MB, reported in the y-axis; as previously stated, those plots are obtained taking the maximum of C' with respect to the Δt axis. The second row shows the accumulation of group delay, reported on the y-axis, with respect to the reference LP_{01} mode. To enhance the visibility of the traces over the effect of local oscillations of the correlation peak, the columns of each subplot in Fig. 2 have been normalized by their mean value; each image has then been normalized to its own maximum. The three columns refer to the target mode groups; distance along the fiber is reported on the x-axis of all the subplots.

To quantify the quality of the correlations, we computed the signal-to-noise ratio (SNR) for the correlation peaks in Fig. 2. The SNR is calculated as the ratio between the normalized correlation peak and the noise floor. The resulting SNR values are approximately 10 for LP_{11}, 5 for LP_{21}, and 8.33 for LP_{02}. These values reflect the strength of the superposition between the backscattered signals of the corresponding modes with the reference mode LP_{01}.

The measured properties were validated against the nominal characteristics of the fiber, as detailed in Table I. This weakly-coupled, step-index FMF was designed to support four robust mode groups (LP_{01}, LP_{11}, LP_{21}, and LP_{02}), with large effective refractive index differences (Δn_{eff}) and DGD between mode groups, as reported in its nominal design in Ref. [8]. Table I provides a comparison of the nominal and measured properties for the mode pairs, highlighting the low mode coupling achieved by the fiber.

TABLE I
COMPARISON BETWEEN THE MEASURED MODAL PROPERTIES AND THE NOMINAL ONES (REF. [8])

Mode Pair	$\boldsymbol{\Delta n_{\text{eff}}}$ **(**$\boldsymbol{\times 10^{-3}}$**)**		**DGD (ps/m)**	
	Nominal	**Measured**	**Nominal**	**Measured**
LP_{01}-LP_{11}	2.3	2.2	4.4	4.5
LP_{01}-LP_{21}	5.1	5.0	8.5	9.0
LP_{01}-LP_{02}	5.9	5.8	7.2	8.6

Table I summarizes the results obtained relative to the LP_{01} mode group. For DGD, the values were calculated as half of the slopes detected in Figs. 2d-f, accounting for round-trip propagation. As previously discussed, any other mode can be used as reference, the only constraint is to correlate signatures of modes that are sufficiently spatially similar. As an example, Fig. 3 shows the results obtained exploiting the LP_{21} mode-group as reference, i.e. setting $LP_{21} \rightarrow LP_{21}$ as $b_1(t)$. The measured values are summarized in table II, showing great consistency with those reported in table I. Nonetheless, it can be readily seen e.g. in Figs. 3c and 3f how the reduced spatial

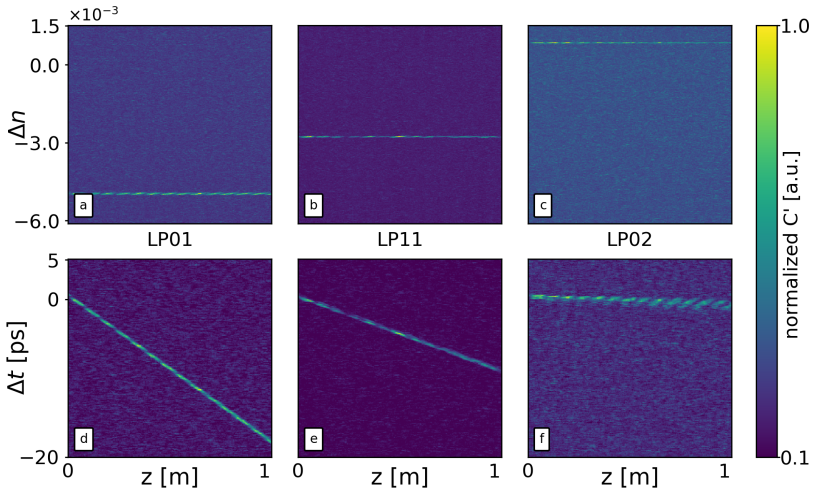

Fig. 3. Modal dispersion properties of the fiber with respect to the LP_{21} mode group. Each column corresponds to a mode group LP_j; the related plots have been obtained from the SCA outcome $C'(t, \Delta t, \Delta f)$ between measurements $LP_{21} \rightarrow LP_{21}$ and $LP_j \rightarrow LP_j$. All the subplots have been derived and normalized as in fig. 2. Modal birefringence and DGD are reported on the y-axis of the first and second row subplots respectively. Distance along the fiber is reported on the x-axis on all the subplots.

TABLE II
MEASURED MODAL DISPERSION WITH RESPECT TO LP_{21}

	LP_{01}	**LP_{11}**	**LP_{02}**
Δn	-5 $\cdot 10^{-3}$	-2.8 $\cdot 10^{-3}$	0.8 $\cdot 10^{-3}$
Δt [ps/m]	-9	-4.5	-0.4

similarity between the correlated LP_{21} and LP_{02} mode groups impacts on the SNR of the analysis, resulting in a reduced contrast. Specifically, the SNR values computed for the LP_{21} reference mode are approximately 6.7 for LP_{21}-LP_{01}, 10 for LP_{21}-LP_{11}, and 4 for LP_{21}-LP_{02}.

V. Detecting Cross-Mode Scattering

In the previous section, we have shown that whenever the SCA is performed among the signatures of two modes LP_i and LP_j, the identified spectral shift $\Delta f_{i,j}$ is related to the refractive index difference $\Delta n_{i,j}$ between the selected modes. In particular, $\Delta f_{i,j}$ is defined as the frequency shift such that the propagation terms of the compared signatures coincide, i.e. such that $-j2\beta_i(f + \Delta f_{i,j}) = -j2\beta_j(f)$. However, this definition holds as long as the propagation term is of the type $\exp(-j2\beta z_k)$; this is true when the forward and backward propagations occur on the same fiber mode. We refer to this kind of signals as to "round-trip" signatures of a certain mode.

In FMFs, cross-mode scattering happens [14]; in this case, the related propagation term becomes $\exp(-j(\beta_i + \beta_j)z_k)$, and the corresponding frequency shift Δf must change accordingly. In particular, when compared to the round-trip signature of mode LP_i, the "mixed" signature involving LP_i and LP_j must lead to a frequency shift Δf such that $-j2\beta_i = -j(\beta_i + \beta_j)$, so that $\Delta f = f_0 \Delta n_{i,j}/(2n_i) = \Delta f_{i,j}/2$. Owing again to the mode selectiveness of the exploited multiplexer, the mixed signatures, if present, should be detected in measurements of the type $LP_i \rightarrow LP_j$, with $i \neq j$.

To verify this, we performed SCA between measurements $LP_i \rightarrow LP_i$ and $LP_i \rightarrow LP_j$. In particular, only one pair of modes has been found to give rise to mixed signatures, namely LP_{01} and LP_{02}. The plots in Fig. 4 report the results obtained comparing the measurements $LP_{01} \rightarrow LP_{01}$ and $LP_{01} \rightarrow LP_{02}$. As expected, the obtained modal birefringence and differential group delay are half of those identified in Figs. 2c and 2f; the results obtained performing SCA between $LP_{01} \rightarrow LP_{01}$ and $LP_{02} \rightarrow LP_{01}$ are similar.

VI. Measuring Relative Chromatic Dispersion

The spatial resolution that can be achieved when measuring coherent Rayleigh backscattering with an OFDR is proportional to the optical bandwidth $\mathcal{B}$ scanned during the acquisition. To achieve high spatial resolution, i.e. small $\delta z = c_0/(2n_0\mathcal{B})$, a typical OFDR scan is performed over a wide optical bandwidth $\mathcal{B}$, usually in the order of several tens of nanometers; as a consequence, the measurement outcome can be affected by the chromatic dispersion of the fiber.

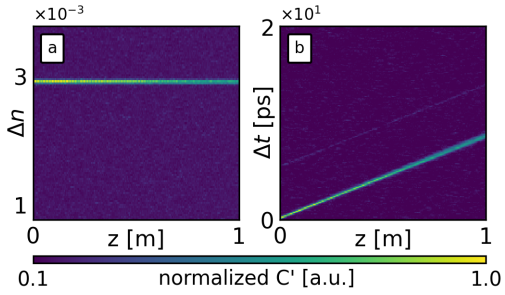

Fig. 4. Evidence of cross-mode scattering in the outcome C' of the SCA performed between measurements $LP_{01} \rightarrow LP_{01}$ and $LP_{01} \rightarrow LP_{02}$. Subplot (a) is obtained as $\max_{\Delta t} C'(t, \Delta t, \Delta f)$; MB is reported on y-axis, while distance along the fiber on x-axis. Subplot (b) is obtained as $\max_{\Delta f} C'(t, \Delta t, \Delta f)$. The delay is reported on y-axis, distance along the fiber is reported on x-axis. The plots have been normalized as in fig. 2.

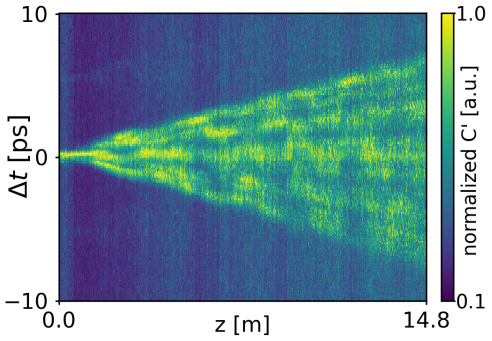

Fig. 5. Effects of chromatic dispersion in the outcome C' of the full-length, full-bandwidth SCA performed between measurements $\mathrm{LP}_{01} \rightarrow \mathrm{LP}_{01}$ and $\mathrm{LP}_{01} \rightarrow \mathrm{LP}_{02}$. The plot is obtained as $\max_{\Delta f} C'(t, \Delta t, \Delta f)$. Delay is reported on the y-axis as the deviation from the corresponding value in table I ,i.e. 8.6 ps/m, while distance along the fiber is reported on the x-axis. The plot has been normalized as in fig. 2.

In terms of delay, the strength of these effects is related to the propagation distance and the OFDR scan bandwidth $\mathcal{B}$, through the dispersion coefficient D_i of the mode LP_i. Whenever the fiber is short enough to make the chromatic dispersion effects fall in the order of the delay resolution δt, the full bandwidth $\mathcal{B}$ can be exploited to obtain the measurements to be analyzed, without introducing detrimental effects, as it was done in Figs. 2 and 3.

However, as the propagation distance increases, the effects of chromatic dispersion become more and more prominent in the measurement's outcome. This is the case of Fig. 5, where the full bandwidth $\mathcal{B} = 8.5$ THz has been exploited to obtain the time (distance) domain coherent backscattering signal of a 14.8-meters long sample of the FMF previously introduced. In particular, the round-trip signatures of modes LP_{01} and LP_{02} have been obtained respectively through the measurement $\mathrm{LP}_{01} \rightarrow \mathrm{LP}_{01}$ and $\mathrm{LP}_{02} \rightarrow \mathrm{LP}_{02}$; SCA has then be performed between the two. For the sake of clarity, the figure reports the measured deviation from the DGD value reported in table I; it can clearly be seen how the delay trace spreads as the propagation distance increases, as a result of the cumulated effects of chromatic dispersion, resulting in a unclear outcome.

The most straightforward way to limit the effects of chromatic dispersion on the SCA is to exploit signatures obtained from a smaller bandwidth $\mathcal{B}_s$, at the cost of an increased spatial sampling step $\delta z_s = c_0/(2n_0\mathcal{B}_s)$. Such signatures can be directly derived from a full-bandwidth measurement of mode LP_i, $b_i(t)$, through pass-band filtering; hereinafter, we refer to the signature obtained from $b_i(t)$ through pass-band filtering over the sub-band $\mathcal{B}_s \subset \mathcal{B}$ as to $b_{i,s}(t)$.

At this point, it is possible to evaluate the effect of chromatic dispersion between modes LP_i and LP_j by partitioning the bandwidth $\mathcal{B}$ in sub-bands $\{\mathcal{B}_s\}_{\{s\in S\}}$ and deriving $b_{i,s}(t)$ and $b_{j,s}(t)$ for each of them. Subsequently, the SCA can be performed between $b_{i,s}(t)$ and $b_{j,s}(t)$, derived from the same sub-band $\mathcal{B}_s$; from the related outcomes C'_s, modal dispersion information can be extracted following the procedure described in section IV.

Figure 6 shows the results for the mode pair (LP_{01}, LP_{02}), whose signatures have been obtained from 4 different 1.5 THz-wide sub-bands $\mathcal{B}_s$, taken from the full measurement bandwidth $\mathcal{B} = 8.5$ THz. The cumulated delay is reported on the y-axis, distance along the fiber on the x-axis. Each subplot a-d corresponds to a sub-band $\mathcal{B}_s$, whose carrier wavelength is reported in the corresponding title. As in Fig. 5, the delay is reported as a deviation from the corresponding value in table I. Looking at the 4 subplots, it can clearly be noted how the detected slope changes according to the considered sub-band.

Repeating the above procedure for all the mode groups, a plot like the one in Fig. 7 can be obtained, where the DGD with respect to the LP_{01} mode group is reported as a function of the sub-band carrier wavelength. In particular, the plot in Fig. 7 reports the DGD per unit length computed considering the maximum cumulated delay, at the fiber end; however, such analysis can be performed at any point along the fiber, thus enabling the distributed characterization of the relative chromatic dispersion between arbitrary pairs of modes. Fig. 8 complements this by reporting the corresponding chromatic dispersion values, derived for each sub-band and mode group relative to LP_{01}. In Figure 8, the chromatic dispersion values for the LP_{21} mode exhibit more pronounced oscillations compared to the other modes (LP_{11} and LP_{02}). This behavior can be attributed to the lower SNR observed in the correlation between the LP_{21} and LP_{01} modes (see Fig. 2). The reduced correlation strength arises from the weaker overlap between the mode field distributions of LP_{21} and LP_{01}, which results in increased noise and wider oscillations in the chromatic dispersion measurements.

As previously introduced, when performing this kind of analysis, a trade-off has to be made between the attainable delay and wavelength resolutions. In particular, exploiting

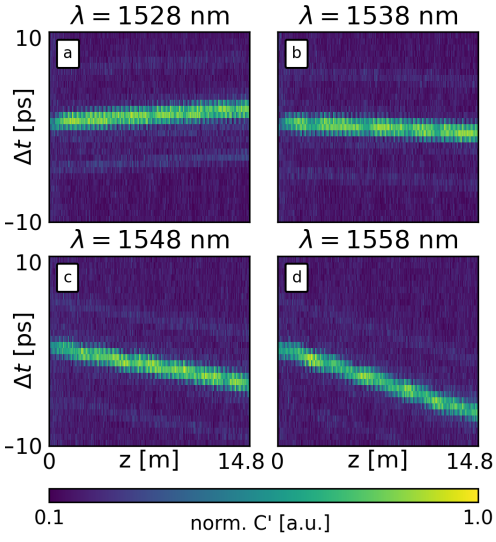

Fig. 6. Evolution of the cumulated group delay between LP_{01} and LP_{02} in 4 different 1.5 THz sub-bands $\mathcal{B}_s$, whose carrier wavelength is reported in the title of the related subplot a-d. Delay is reported on the y-axis as the deviation from the corresponding value in table I, i.e. 8.6 ps/m, while distance along the fiber is reported on the x-axis. Each subplot a-d has been obtained as $\max_{\Delta f} C'_s(t, \Delta t, \Delta f)$ from the related SCA outcome C'_s and has been normalized as in fig. 2.

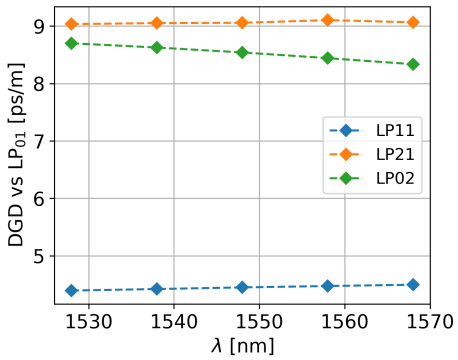

Fig. 7. Effects of chromatic dispersion: DGD computed for each LP mode group with respect to the LP_{01} as a function of the sub-band carrier wavelength

smaller sub-bands enables a more careful characterization of the evolution of the DGD along the wavelength axis. On the other hand, smaller sub-bands lead to worse delay resolution δt. In this case, we exploited 1.5 THz sub-bands to get 5 wavelength points along the full 8.5 THz bandwidth $\mathcal{B}$, providing a delay resolution δt equal to 0.67 ps. The increased sampling step δt affects also the attainable spatial resolution through the window length L, which must be sufficiently long (in terms of samples) to provide the necessary SNR when performing correlations. In this case, it was set to 512 samples, leading to $L \simeq 3.5$ cm.

VII. Conclusions

In this paper, we have shown how to perform a spatially-resolved measure of modal and chromatic dispersion between arbitrary pairs of modes of a weakly-coupled FMF, obtained through a proper analysis of its Rayleigh backscattering traces. Relying on a high-resolution OFDR, the method cannot be straightforwardly extended to fiber lengths beyond few hundreds of meters, thus being indicated for laboratory characterization of fibers. Currently, the analysis focuses only on the positions (in terms of differential delay Δt and frequency shift Δf) of the correlation peaks, neglecting their amplitude. However, we believe that these amplitudes may provide quantitative information about the mode coupling; yet, the development of an appropriate model to interpret the data will be the object of future studies. Nonetheless, the analysis provides values in very good agreement with the nominal ones with centimeter-scale spatial resolution and sub-picosecond delay resolution.

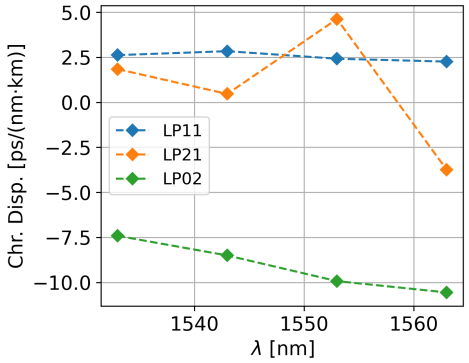

Fig. 8. Chromatic dispersion values computed for each LP mode group relative to the LP_{01} mode group, plotted as a function of the sub-band carrier wavelength.

Acknowledgment

The authors are thankful to Prysmian for providing the fiber sample. This work is partially supported by the European Union under the Italian National Recovery and Resilience Plan (NRRP) of NextGenerationEU, partnership on "Telecommunications of the Future" (PE0000001- program "RESTART") and by MIUR (PRIN 2017, project FIRST).

References

[1] S. Mechels, J. Schlager, and D. Franzen, "High-resolution differential-mode delay measurements in optical fibers using a frequency-domain phase-shift technique," *IEEE Photonics Technology Letters*, vol. 9, no. 6, pp. 794–796, Jun. 1997.

[2] J. Y. Lee and D. Y. Kim, "Determination of the differential mode delay of a multimode fiber using Fourier-domain intermodal interference analysis," *Optics Express*, vol. 14, no. 20, pp. 9016–9021, Oct. 2006.

[3] N. K. Fontaine, R. Ryf, M. A. Mestre, B. Guan, X. Palou, S. Randel, Y. Sun, L. Grüner-Nielsen, R. V. Jensen, and R. Lingle, "Characterization of space-division multiplexing systems using a swept-wavelength interferometer," in *2013 Optical Fiber Communication Conference and Exposition and the National Fiber Optic Engineers Conference (OFC/NFOEC)*, Mar. 2013, pp. 1–3.

[4] X. Chen, J. E. Hurley, J. S. Stone, and M.-J. Li, "Chromatic dispersion measurements of single-mode fibers, polarization-maintaining fibers, and few-mode fibers using a frequency domain method," *Photonics*, vol. 10, no. 2, 2023.

[5] R. Veronese, M. Santagiustina, A. Galtarossa, and L. Palmieri, "Experimental characterization of perturbation-induced modal birefringence in few-mode fibers," in *45th European Conference on Optical Communication (ECOC 2019)*, 2019, pp. 1–4.

[6] S. Ohno, K. Toge, D. Iida, and T. Manabe, "Distributed spatial mode dispersion measurement along strongly coupled multicore fibers based on the correlation analysis of rayleigh backscattering amplitudes," *Opt. Express*, vol. 25, no. 24, pp. 29 650–29 658, Nov 2017. [Online]. Available: https://opg.optica.org/oe/abstract.cfm?URI=oe-25-24-29650

[7] R. Veronese, A. Galtarossa, and L. Palmieri, "Distributed characterization of few-mode fibers based on optical frequency domain reflectometry," *Journal of Lightwave Technology*, vol. 38, no. 17, pp. 4843–4849, 2020.

[8] P. Sillard, M. Bigot-Astruc, D. Boivin, H. Maerten, and L. Provost, "Few-mode fiber for uncoupled mode-division multiplexing transmissions," in *2011 37th European Conference and Exhibition on Optical Communication*, Sep. 2011, pp. 1–3, iSSN: 1550-381X.

[9] M. E. Froggatt and D. K. Gifford, "Rayleigh backscattering signatures of optical fibers—Their properties and applications," in *2013 Optical Fiber Communication Conference and Exposition and the National Fiber Optic Engineers Conference (OFC/NFOEC)*, Mar. 2013, pp. 1–3.

[10] M. Nakazawa, "Rayleigh backscattering theory for single-mode optical fibers," *J. Opt. Soc. Am.*, vol. 73, no. 9, pp. 1175–1180, Sep 1983.

[11] A. J. Rogers and V. A. Handerek, "Frequency-derived distributed optical-fiber sensing: Rayleigh backscatter analysis," *Applied Optics*, vol. 31, no. 21, p. 4091, Jul. 1992.

[12] M. E. Froggatt, D. K. Gifford, S. Kreger, M. Wolfe, and B. J. Soller, "Characterization of Polarization-Maintaining Fiber Using High-Sensitivity Optical-Frequency-Domain Reflectometry," *Journal of Lightwave Technology*, vol. 24, no. 11, pp. 4149–4154, Nov. 2006.

[13] A. M. Velazquez-Benitez, J. C. Alvarado, G. Lopez-Galmiche, J. E. Antonio-Lopez, J. Hernández-Cordero, J. Sanchez-Mondragon, P. Sillard, C. M. Okonkwo, and R. Amezcua-Correa, "Six mode selective fiber optic spatial multiplexer," *Optics Letters*, vol. 40, no. 8, p. 1663, Apr. 2015.

[14] Z. Wang, H. Wu, X. Hu, N. Zhao, Q. Mo, and G. Li, "Rayleigh scattering in few-mode optical fibers," *Scientific Reports*, vol. 6, no. 1, p. 35844, 2016.